RSC Advances

PAPER

View Article Online
View Journal | View Issue

Cite this: *RSC Adv.*, 2023, **13**, 3602

Thermal analysis of novel third-generation phase-change materials with zinc as a chemical modifier

Vishnu Saraswat,[a] Shiv Kumar Pal,[a] N. Mehta, *[a] Arun Kumar[b] and M. M. A. Imran[c]

Received 6th November 2022
Accepted 7th January 2023

DOI: 10.1039/d2ra07041c

rsc.li/rsc-advances

The thermal analysis in the present work is done to analyze the glass/crystal phase transformation in a newly synthesized glassy system (*i.e.*, glassy SeTeSnZn alloys) consisting of chalcogenides Se and Te as major elements, Sn as a third element of the parent alloy and Zn as a chemical modifier. The role of increasing the Zn concentration at the cost of Se has been understood by correlating the kinematics of structural relaxation during the glass transition phenomenon and devitrification during the crystallization phenomenon in the chalcogenide glasses (ChGs) of the quaternary STSZ [*i.e.*, $Se_{78-x}Zn_xTe_{20}Sn_2$ ($0 \leq x \leq 6$)] system and their different physicochemical properties. A noticeable rise in the crystallization rate is observed after the addition of Zn in the parent SeTeSn glass. With the rise in the zinc content, the values of average heat of atomization and overall mean bond energy are found to be decreased with the decrease in cohesive energy of samples. An inverse correlation is observed between the thermal stability parameter and the enthalpy released during the glass/crystalline phase transformation.

1. Introduction

In recent years, the use of zinc as a dopant or metallic modifier in different advanced functional materials has been enhanced[1–6] because of its efficient role in controlling the properties of the parent materials and achieving fascinating and fruitful results. The zinc chalcogenides have attracted the attention of experimentalists working on metal chalcogenides because of their robust bonding, large energy gaps, high enthalpies of formation, and melting points as compared to most of the other metallic chalcogenides formed by using other elements placed in the II–VI.[1–10] The crystal dynamics of zinc chalcogenides[4–6] suggest their utilization in various applications.[4–10] Particularly, the recent literature survey of the last decade reveals that zinc is one of the building elements of phase change materials (PCMs) for use in phase change optical memory.[11–17] These features compelled various research groups to utilize Zn as a modifier for preparing multicomponent (binary and ternary) ChGs.[18–35]

Mehta *et al.*[18] compared the effective values of thermal diffusivity and corresponding thermal conductivity of binary $Se_{90}Zn_{10}$ and $Te_{90}Zn_{10}$ alloys and found that both parameters are lower for $Se_{90}Zn_{10}$ alloy as compared to $Te_{90}Zn_{10}$ alloy. The outcome of Zn addition on the number of defect states per unit volume in the parent $Se_{70}Te_{30}$ sample was analyzed by Srivastava *et al.*[19] by performing a.c. conductivity measurements.

Singh *et al.*[20,21] observed the Meyer–Neldel relation between the rate constant and activation energy in thermally controlled crystallization during the calorimetric studies of ternary Se–In–Zn glasses. Nasir *et al.*[22] reported the thermal analysis of the kinematics of glass transition as well as the recrystallization of binary $Se_{98-x}Zn_x$ glasses. They noticed the significant impact of zinc on the glass/crystal phase transformation of selenium glass. Nasir and Zulfequar[23,24] performed the electrical measurement too in these glasses to estimate the number of localized states per unit volume and their dielectric behavior. They found the enhancement in the corresponding number density when the concentration of Zn content rises in the selenium glass. They also noticed a sufficient dielectric dispersion as a consequence of Zn incorporation.

The thermophysical and optical characterization of ternary $Se_{98-x}In_xZn_2$ and $Se_{93-x}Te_5In_xZn_2$ ($0 \leq x \leq 10$) was done by Singh[25,26] for the comparison between these ternary and quaternary samples. Kishore *et al.*[27] used FTIR spectra of ternary $Se_{72-x}S_{28}Zn_x$ ($0 \leq x \leq 4$) for analyzing the influence of Zn on the optical parameters of parent $Se_{72}S_{28}$ glass and observed the significant decrement in the optical gap by a small rise in the content of zinc. Ahmad *et al.*[28] used silver ion radiation to expose amorphous thin films of the SeSZn sample and investigated the irradiation effect on optical, electrical, and structural properties. Abbady *et al.*[29] compared the effect of Zn over two other additives (Ge and Ga) on the optical linearity/non-linearity of selenium by preparing thin-film samples. They found that most of the linear/non-linear optical parameters are optimized for the addition of Zn.

Alwany *et al.*[30] reported the optical properties of ternary $Ge_{20}Se_{70}Zn_{10}$ alloy by preparing its amorphous thin film. Lu

[a]Physics Department, Banaras Hindu University, Varanasi-221005, India. E-mail: dr_neeraj_mehta@yahoo.co.in
[b]Physics Department, IIT Roorkee, Roorkee-247667, India
[c]Physics Department, Al-Balqa Applied University, Al-Salt-19117, Jordan

et al.[31] designed a novel $(As_2S_3)_{100-x}(ZnSe)_x$ $(0 \leq x \leq 30)$ system for the possible applications in Mid-IR fiber lasers and found that these materials show compatibility with a drawing scheme adopted for preparing fibers showing low-loss of signals. Azhniuk and his research group[32] observed the sign of photoinduced creation of ZnSe nano-crystallites during the investigation of the optical characterization of As_2Se_3 thin films doped with zinc.

Nagpal *et al.*[33] investigated the consequences of adding zinc to the various optical parameter of binary $Se_{90}Sb_{10}$ glass $(0 \leq x \leq 10)$ and concluded that the optical properties changed noticeably. Chazot and his research team[34] tried to design a fiber laser by using a composite that consists of active crystals of Fe:ZnSe in a glass matrix. For this, they checked the suspension stability of zinc selenide crystals in a specific glass made of As_2S_3 and As_2Se_3 having compositions 94.6 and 5.4 respectively. Some glass ceramics of the ternary Se–Ge–Zn system were developed by Velea *et al.*[35] for applications in infrared optics that were found capable of the prospective research work in IR optics.

In this way, different groups used zinc as a modifier in various multicomponent ChGs (especially binary and ternary systems) to see its consequence on the physical properties of parent samples. The above literature survey reveals that only a few endeavors were done to study the role of Zn on different physical properties in quaternary systems of ChGs. Keeping in mind this point and the fascinating results reported by the above research groups, we decided to synthesize some ChGs of the quaternary SeTeSnZn system. In this paper, we have reported a systematic analysis of the outcomes derived from the calorimetric experiments done on the present samples of the quaternary STSZ system.

2. Experimental

For the present studies, we prepared some glassy samples of SeTeSnZn by quenching their melts in chilled water. The specifics of this synthesis technique are described in ref. 36–38. The non-crystalline character of as-prepared samples was confirmed by the X-ray diffraction (XRD) technique and analysis of scanning electron microscopic (SEM) pictures. Fig. 1 shows such results for as-prepared samples. There were no sharp peaks of sufficient intensity in the XRD patterns of the present samples. Only a few weak peaks of insignificant intensities were observed over the broad humps *i.e.*, the first sharp diffraction peak (FSDP) and second sharp diffraction peak (SSDP) [see Fig. 1(a)] that were the characteristic of intermediate-range ordering in the present samples. However, we have identified some distinguished peaks that can be indexed.

The primary peaks of crystalline t-Se *i.e.*, trigonal Se (COD-9008579) are visible at 2θ values of 23.5°, 29.7°, and 51.7°, which correspond to the crystal planes (100), (101), and (201), respectively while the small peaks at 23.05°, 27.55°, 45.88°, 47.04°, and 49.69° are, respectively, associated with the crystal planes (100), (101), (003), (200), and (201) of crystalline t-Te *i.e.*, trigonal Te. The diffraction peaks at 2θ of 32°, are compared with the JCPDS data and respectively indexed to the

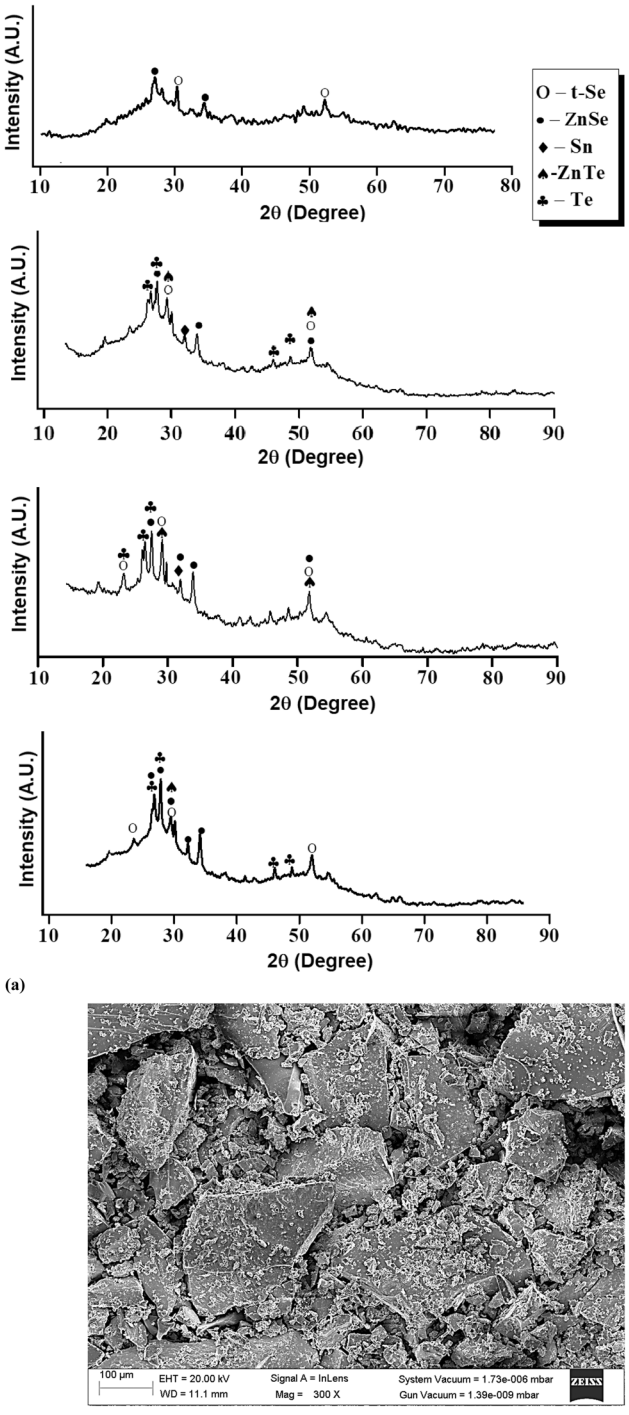

Fig. 1 (a) XRD patterns of the as-prepared samples indicate the glassy nature with evidence of some crystallites embedded in the glass matrix of the samples. (b) SEM picture of a representative sample ($x = 2$) for the confirmation of the glassy nature.

crystallographic planes (101) polycrystalline planes metallic tin (JCPDS card no. 004-0673). Further, the peaks at (2θ) 27.65, 45.13, and 52.6 in the ZnSe spectrum correspond to the index planes (111), (220), and (311) for cubic zinc mix structured ZnSe (JCPDS card no. 65-9602). In addition to these peaks, the ZnSe

diffraction pattern also shows peaks at (2θ) 23.55, 26.4, 28.6, 30.5, 34.9, and 43.8, which correspond to the Miller indices (111), (100), (002), (101), (102) and (220). ZnTe nanocrystals' diffraction peaks at 29.92, 49.52, and 51.88 could be correlated with the (200), (311), and (222) planes of the cubic-phase ZnTe.

Further, no sign of crystallinity was observed in the SEM picture of the as-prepared samples. Such an SEM picture of a representative sample of $Se_{76}Te_{20}Sn_2Zn_2$ is shown here [see Fig. 1(b)]. For the thermal characterization of the samples, we adopted non-isothermal heating and performed the calorimetric measurements in a differential scanning calorimeter (TA Instruments, USA; Model: Q20). DSC runs were performed at four diverse heating rates for all the samples. For doing calorimetric measurement in the DSC unit, the samples were crushed and 5 mg powder of each sample was enclosed in the crimped pans. For the calibration of the DSC cell, indium was used. Nitrogen gas is used as purge gas during the calorimetric measurements. The sensitivity of the employed DSC unit was 1.0 μW and temperature accuracy was ±0.1 °C. The full details of this technique are described in ref. 39.

3. Results and discussion

Fig. 2 shows the results of the calorimetric experiment performed on the samples of the STSZ glassy system at a specific heating rate of 10 K min^{-1}. The appearance of distinct glass transition and crystallization phenomena are seen as the first endothermic peak and the second exothermic peak in each scan of this figure. Further, the homogeneity of each as-prepared sample is reflected in the sharpness of the glass transition and crystallization peaks. When the homogeneity of the samples is poor, there is a strong chance of phase separation,[40–43] which appears as the splitting of the glass transition peak and/or crystallization peak in double or triple components or the broadening of its width.

Abdel-Wahab[43] prepared a ternary glass ($Se_{77.5}Te_{20}Sn_{2.5}$) whose composition was almost identical to the parent glass ($Se_{78}Te_{20}Sn_2$) of the present SeTeSnZn system. He performed DSC experiments in $Se_{77.5}Te_{20}Sn_{2.5}$ and found that this sample had two exothermic crystallization peaks as a signature of phase separation. However, such splitting of the glass transition peak and/or crystallization peak is neither observed in the parent $Se_{78}Te_{20}Sn_2$ ternary glass nor zinc containing SeTeSnZn quaternary glasses. Thus, in our samples, the chance of this unwanted situation is ruled out as a signature of the sharpness of the glass transition peaks. Similar observations were observed in DSC scans obtained by calorimetric measurements at other heating rates. From such DSC scans of all samples at different heating rates, we have determined the glass transition temperature T_g and the crystallization temperature T_c by noting down the temperatures corresponding to peak maximum.

To realize the dependency of these characteristic temperatures on heating rate β, we have used the following empirical relations suggested by Lasocka:[44]

$$T_g = A_g + B_g \log \beta \quad (1)$$

Here A_g, and B_g are Lasocka's parameters for glass transition.

The intercept A_g in eqn (1) represents the theoretical value of T_g corresponding to 1 K min^{-1} heating rate. Lasocka's parameter B_g represents the slope of the straight line shown by eqn (1). Such linear graphs are shown in Fig. 3. Table 1 tabulates the value of A_g and B_g for the present samples.

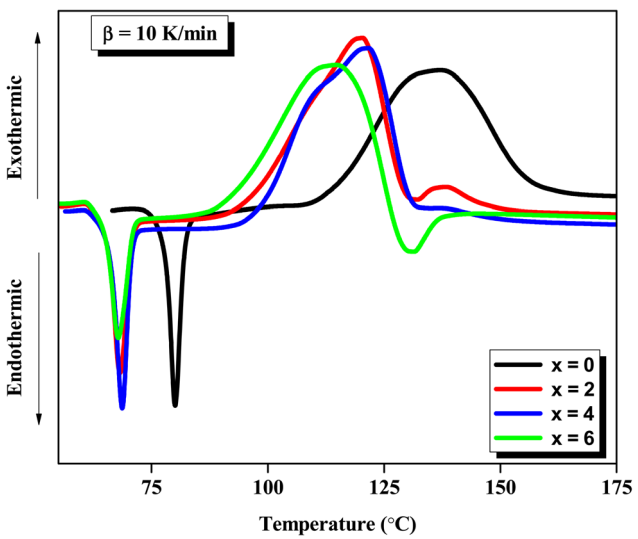

Fig. 2 DSC scans of samples (x = 0, 2, 4, 6) of glassy system $Se_{78-x}Zn_xTe_{20}Sn_2$ at a particular heating rate (10 °C min^{-1}) represent sharp endothermic peaks as a sign of thermal relaxation in the glass transition region.

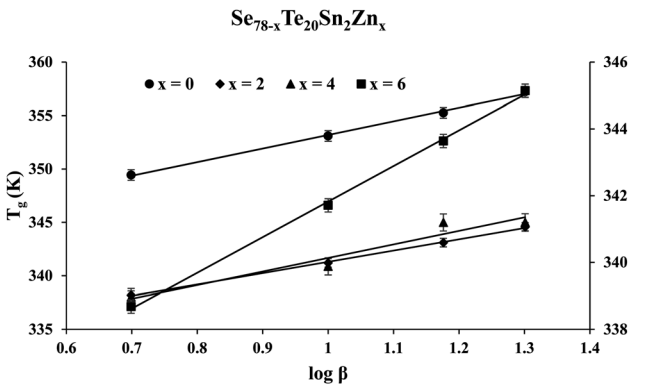

Fig. 3 Plots of T_g *versus* log β for the present samples. The secondary y-axis is plotted for x = 6.

Table 1 Values of Lasocka's parameters of glass transition (*i.e.*, A_g, B_g) and crystallization (*i.e.*, A_c, B_c) for present samples

Sample	A_g (K)	B_g (min^{-1})	A_c (K)	B_c (min^{-1})
$Se_{78}Te_{20}Sn_2$	340.5	12.7	380.7	29.1
$Se_{76}Te_{20}Sn_2Zn_2$	330.7	10.6	372.5	20.6
$Se_{74}Te_{20}Sn_2Zn_4$	329	12.7	364.7	22.2
$Se_{72}Te_{20}Sn_2Zn_6$	331.1	10.7	370.9	23.3

The similar empirical relation of T_c for crystallization phenomenon can be expressed in terms of β:[44]

$$T_c = A_c + B_c \log \beta \quad (2)$$

Here A_c, and B_c are Lasocka's parameters for crystallization. The linear graphs corresponding to eqn (2) are shown in Fig. 4 for the present glasses. Table 1 tabulates the value of A_c and B_c for the present samples.

To find the correlation between T_g and T_c in the present study, we have derived the following relation by using eqn (1) and (2):

$$T_g = \left(\frac{B_c A_g - A_c B_g}{B_c}\right) + \left(\frac{B_g}{B_c}\right) T_c \quad (3)$$

Eqn (3) reveals that the kinetic temperatures T_c and T_g, corresponding to the crystallization and glass transition phenomena respectively, are mutually dependent on each other. Another interesting fact about such correlation is that we can use this equation for the determination of Kauzmann temperature (T_k) which is a significant parameter for the characterization of glassy materials from a thermodynamic lookout.[45] The T_k represents the value of temperature upon which the entropy of a liquid having glass-forming ability becomes equal to that of its crystalline complement. Thus, keeping in mind the thermodynamic aspects, it signifies a lower limit for T_g below which the presence of an under-cooled glass-forming liquid does not obey thermodynamic law.[45] We can use eqn (3) for the determination of the Kauzmann temperature in the present case by keeping in mind that the Kauzmann temperature is the bottommost hypothetical borderline for the glass transition corresponding to a permissible assumption $T_g = T_c = T_k$[46] at a particular heating rate β_k (known as Kauzmann heating rate).

Solving eqn (3) for T_k (which is equal to T_g or T_c) and β_k, we obtain the following relations:

$$T_k = \left(\frac{B_c A_g - A_c B_g}{B_c}\right) \quad (4)$$

and

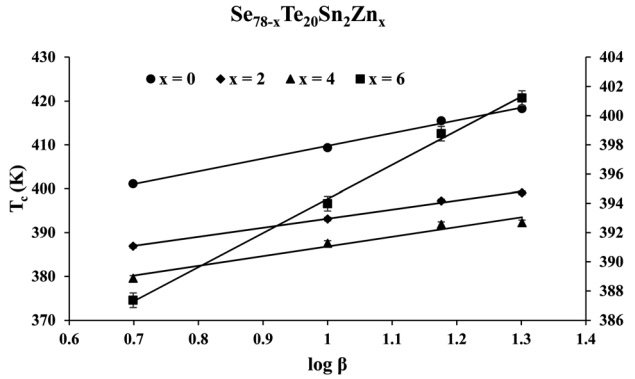

Fig. 4 Plots of T_c *versus* log β for the present samples. The secondary y-axis is plotted for $x = 6$.

Table 2 Values of Kauzmann's parameter (*i.e.*, T_k, β_k) for present samples

Sample	T_k (K)	β_k (K min^{-1})
$Se_{78}Te_{20}Sn_2$	309.1	2.12×10^{-6}
$Se_{76}Te_{20}Sn_2Zn_2$	286.7	2.7×10^{-10}
$Se_{74}Te_{20}Sn_2Zn_4$	281.2	2.2×10^{-9}
$Se_{72}Te_{20}Sn_2Zn_6$	297.9	5.8×10^{-8}

$$\beta_k = 10^{\left[\frac{A_g - A_c}{B_c - B_g}\right]} \quad (5)$$

Table 2 tabulates the values obtained for T_k and β_k from eqn (4) and (5) in the present case. From this table, one can realize that it is enormously hard to perform the calorimetric experiments to detect this ideal glass transition because of the very low values of the heating rate.

The composition dependence of different kinetic parameters indicates that there is non-linear variation in different parameters. ChGs are famous for their non-linear physical properties due to their inherent structural flexibility. In ChGs, earlier it was believed that only two critical compositions are having the values 2.4 and 2.67 of mean coordination number ($\bar{Z}$) in the IV–VI chalcogenide glassy system at which such a reversal in the compositional trend of different physical properties is observed. However, we have observed such a reversal in the compositional trend of Lasocka's parameters and Kauzmann's parameters at lower values of $\bar{Z}$. In the recent study,[47–49] it has been proposed that the rigidity percolation transition (*i.e.*, a reversal in the compositional trend) can occur over a range of mean coordination numbers leading to three distinct phases namely; floppy, intermediate and rigid. Various researchers[50–52] reported that such transitions occur at different compositions for different physical properties even at lower values of $\bar{Z}$. This is probably the reason behind the observation of the reversal in the compositional trend of Lasocka's parameters and Kauzmann's parameters at different compositions.

Moynihan and coworkers[53] developed a method to evaluate the glass transition activation energy. This relation is generally known as the Moynihan relation and can be expressed as:

$$\ln(\beta) = \left(-\frac{E_g}{RT_g}\right) + \text{constant} \quad (6)$$

Although the Kissinger equation[54] is primarily derived for the evaluation of kinetic activation energy E_c involved in thermally governed crystallization, one can adopt an analogous relation for the glass transition to estimate the corresponding activation energy E_g. The premise of employing this relation for the assessment of E_g originates from the shifting of maxima at T_g towards the higher temperature side with the rise in β values. Consequently, the analogous Kissinger equation takes the form:[54]

$$\ln\left(\frac{\beta}{T_g^2}\right) = -\frac{E_g}{RT_g^2} + \text{constant} \quad (7)$$

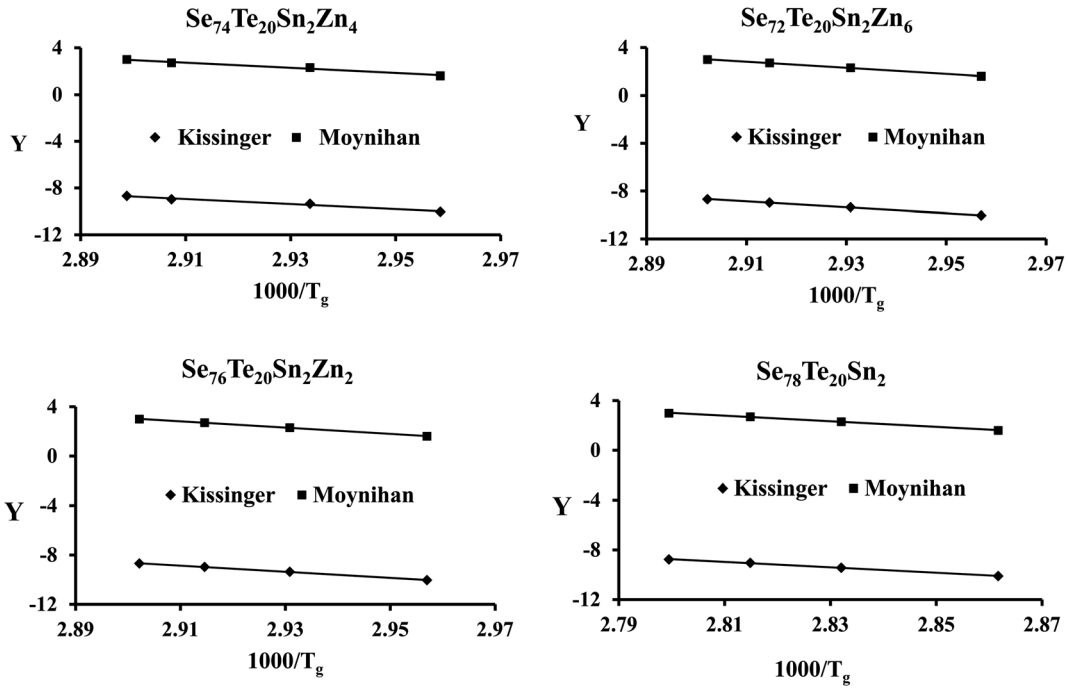

Fig. 5 Plots of $\ln(\beta)$ *vs.* $10^3/T_g$ and $\ln(\beta/T_g^2)$ *vs.* $10^3/T_g$ for the present samples. On the y-axis, $Y = \ln(\beta)$ and $\ln(\beta/T_g^2)$ for the Moynihan method and Kissinger method, respectively.

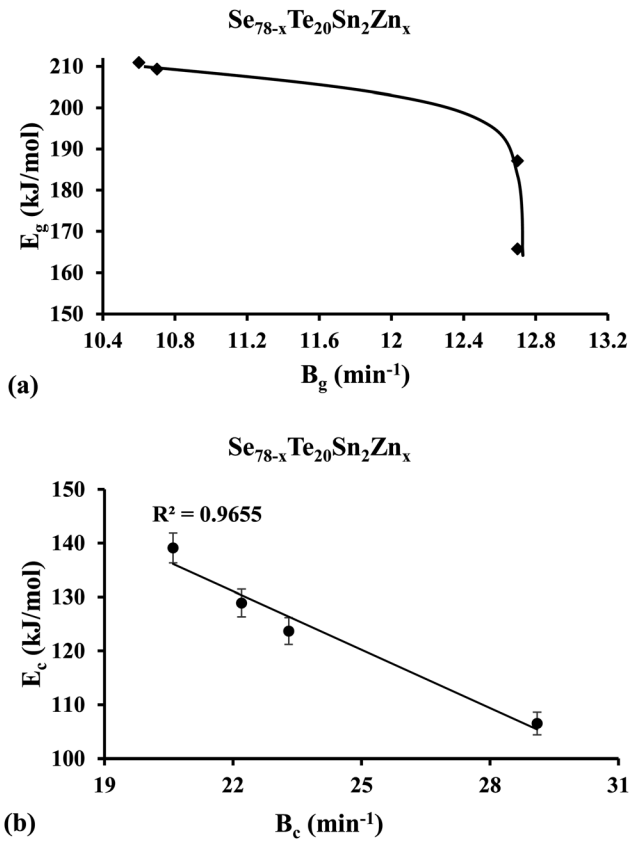

Fig. 6 Plots of (a) glass transition activation energy E_g against Lasocka parameter B_g, and (b) crystallization activation energy E_c against Lasocka parameter B_g.

The plots of $\ln(\beta)$ and $\ln(\beta/T_g^2)$ against $1000/T_g$ are shown in Fig. 5. The linear nature of the graphs confirms the applicability of eqn (6) and (7). From the gradients of such linear graphs, we have determined E_g for all the samples.

Lasocka[44] observed that B_g is subject to the cooling rate of the melt unswervingly. He suggested that parameter B_g signifies the retroactivity of the configurational alterations arising in the vicinity of the temperature range corresponding to the glass transformation. Keeping in mind the fact that glass transition activation energy E_g is related to the movements of structural species throughout the thermal relaxation in the neighborhood of the glass transition, we have plotted the graph of E_g against parameter B_g and found that E_g of the samples is decreased non-linearly with increasing parameter B_g [see Fig. 6(a)] in the present case. This indicates that the higher the value of B_g, the more transient responsiveness of the local configurational deviations and so the glass network requires less activation energy. A similar correlation between glass transition activation energy E_g and Lasocka parameter B_g was observed earlier in the glassy $Se_{80-x}Te_{20}Sn_x$ system by Kumar *et al.*[55] Thus, our present results of the glassy $Se_{80-x}Te_{20}Sn_2Zn_x$ system are consistent with our previous results of the glassy $Se_{80-x}Te_{20}Sn_x$ system.[55]

By using the JMA model, various methods are developed by different authors to calculate E_c for different kinds of glasses. As derived by Kissinger,[54] we can express E_c in terms of β as follows:

$$\ln\left(\frac{\beta}{T_c^2}\right) = -\frac{E_c}{RT_c^2} + \text{constant} \quad (8)$$

Matusita and Sakka[56,57] set up the following equation for the determination of E_c from the classical JMA relation:

$$\ln(\beta) = -\frac{E_c}{RT_c} + \text{constant} \quad (9)$$

Augis and Bennett[58] derived a slightly different non-isothermal relation to calculate the crystallization activation energy:

$$\ln\left(\frac{\beta}{T_c}\right) = -\frac{E_c}{RT_c} + \ln K_0 \quad (10)$$

By using eqn (8)–(10) we have plotted the graphs of $\ln(\beta/T_c^2)$ [*i.e.*, Kissinger method], $\ln(\beta)$ [*i.e.*, Matusita–Sakka method] and $\ln(\beta/T_c)$ [*i.e.*, Augis–Bennett method] against $1000/T_c$. Such plots are shown in Fig. 7. By using the slopes of these graphs, we have evaluated the E_c values in the present study for the various samples. Keeping in mind the observed correlation between Lasocka parameter B_g and glass transition activation energy E_g, we have plotted a similar plot for the Lasocka parameter B_c and crystallization activation energy E_c and observed that E_c is also decreased with a rise in Lasocka parameter B_c [see Fig. 6(b)]. However, the decrement in E_c with B_c is almost linear.

The crystallization rate of ChGs can be determined by studying its temperature dependence which is governed by the Arrhenius equation:[59,60]

$$K = K_0 \exp\left(-\frac{E_c}{R\,T}\right) \quad (11)$$

Since the rate K represents the growth rate of the crystalline species during the devitrification of the samples, we can understand the influence of zinc incorporation on the rate constant K of crystallization for the parent glass by substituting the value of the crystallization activation energy E_c in eqn (11) at the temperatures lying in the crystallization region of the SeTeSnZn samples.

Knowing the value of E_c and pre-factor K_0, we have determined the rate of crystallization for the present samples of the SeTeSnZn system using eqn (11). The composition dependence of ln K is shown in Fig. 8 for all the samples at different heating rates. From this figure, we see that the crystallization rate of the quaternary alloys is larger in comparison to parent SeTeSn glass and it attains an almost constant higher value after zinc incorporation at all the heating rates.

We have used the following relation for the determination of the average heat of atomization $\bar{H}_A$ of the samples in the present study:[61]

$$\overline{H}_A = \frac{(jH_{Se} + kH_{Te} + lH_{Sn} + mH_m)}{(j+k+l+m)} \quad (12)$$

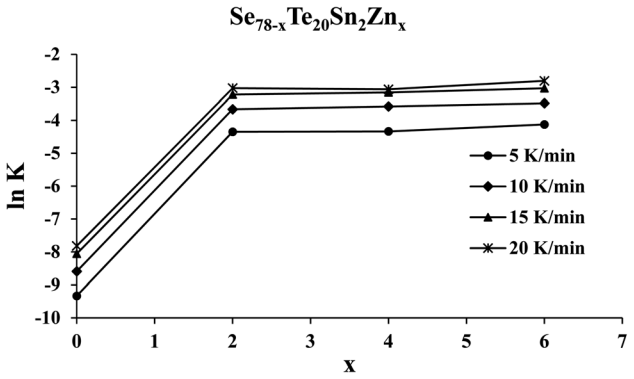

Fig. 8 Composition dependence of the rate of crystallization K.

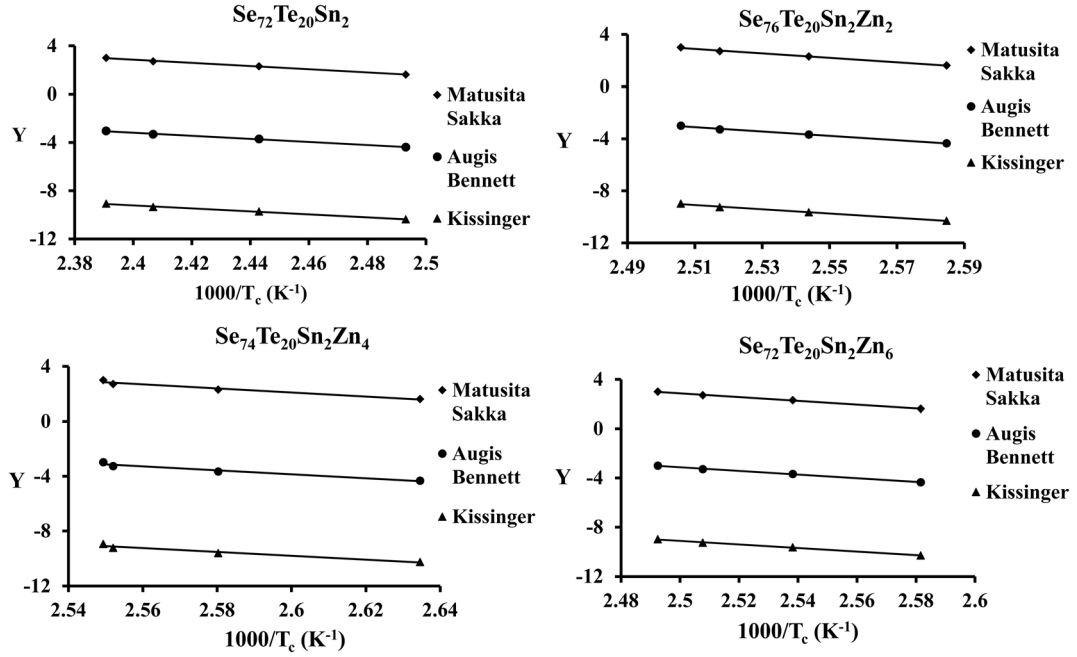

Fig. 7 Plots of $\ln(\beta/T_c^2)$, $\ln(\beta)$, and $\ln(\beta/T_c)$ *versus* $1000/T_c$ for the present samples. On the y-axis, $Y = \ln(\beta/T_c^2)$, $\ln(\beta)$, and $\ln(\beta/T_c)$ for the Kissinger method, Matusita–Sakka method, and Augis–Bennett method respectively.

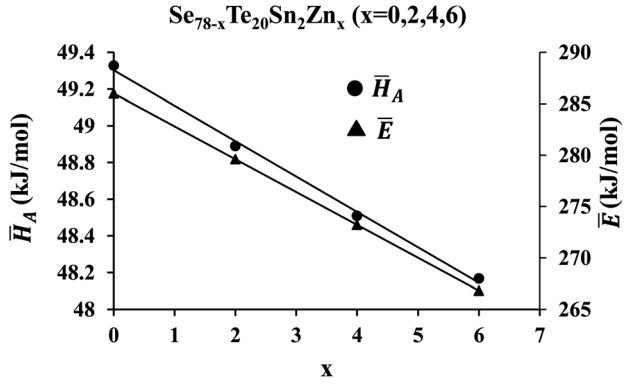

Fig. 9 Composition dependence of average heat of atomization $\bar{H}_A$ and overall mean bond energy $\bar{E}$.

Here H_{Se}, H_{Te}, H_{Sn}, and H_{Zn} are the respective atomization heat values of Se, Te, Sn, and Zn in the present samples ($0 \leq x \leq 6$) of the $Se_{78-x}Zn_xTe_{20}Sn_2$ system, while j, k, l, and m are the corresponding concentrations. The dependency of $\bar{H}_A$ on the zinc content is revealed in Fig. 9.

To determine the overall mean bond energy of the samples, we have used a model recommended by Tichy and Ticha based on the approach chemical bond theory.[62] According to the Tichy–Ticha model, the ChGs can be categorized into three categories based on a parameter R according to the following conditions:

$$R = 1;\ R > 1 \text{ or } R < 1 \tag{13}$$

For R is equal to one (*i.e.*, $R = 1$), Tichy and Ticha suggested that the glass network attains the stoichiometric composition because of the presence of heteropolar bonds solitary and this composition is corresponding to the chemical threshold where we observe frequently the utmost values of glass transition temperature T_g. If R is greater than one (*i.e.*, $R > 1$), then the corresponding glassy system will be a member of the chalcogen-rich family. In such a case, the glassy system consists of both chalcogen–chalcogen bonds and heteropolar bonds. If R is smaller than one (*i.e.*, $R < 1$), then the corresponding glassy system will be a member of the chalcogen-poor family. In such cases, the chalcogen–chalcogen bonds are almost absent and the glassy system consists of only metal–metal bonds and heteropolar bonds.[62] Since in the present studies, the concentration of chalcogen elements Se and Te is very high as compared to the other two elements (Sn and Zn), our glassy system belongs to the chalcogen-rich family.

For the chalcogen-rich region, the Tichy–Ticha model further suggests that the degree of cross-linking can be determined by using the expression:

$$P_r = \frac{kN_{Te} + lN_{Sn} + mN_{Zn}}{(k + l + m)} \tag{14}$$

In eqn (14), N_{Zn}, N_{Sn}, and N_{Te} are the respective coordination numbers of Zn, Sn, and Te. The average bond energy (E_c) corresponding to the mean cross-linking per atom is given by:[62]

$$E_c = P_r \times E_{hb} \tag{15}$$

Here, E_{hb} is the mean hetero-polar bond energy that can be expressed as:[62]

$$E_{hb} = \frac{kN_{Te}(E_{Se-Te}) + lN_{Sn}(E_{Se-Sn}) + mN_{Zn}(E_{Se-Zn})}{(kN_{Te} + lN_{Sn} + mN_{Zn})} \tag{16}$$

In eqn (16), E_{Se-Te}, E_{Se-Sn}, and E_{Se-Zn} represent the hetero-polar bond energies of Se atoms with Te, Sn, and Zn atoms respectively. For the 'remaining glass matrix', we now express the mean bond energy per atom E_{rm} as follows:[62]

$$E_{rm} = \frac{(E_{Se-Se}) \times (\bar{r} - 2P_r)}{\bar{r}} \tag{17}$$

In eqn (17) E_{Se-Se} represents the strength of the homopolar Se–Se bond in the chalcogen-rich region.

Knowing the values of E_c and E_{rm}, we can determine the overall value $\bar{E}$ of mean bond energy by adding them, *i.e.*,:[62]

$$\bar{E} = E_c + E_{rm} \tag{18}$$

Fig. 9 shows the dependency of $\bar{E}$ on the concentration of zinc also. This figure reveals that both average heat of atomization $\bar{H}_A$ and overall mean bond energy $\bar{E}$ are decreased with the intensification of the zinc atoms in the parent SeTeSn glass. This is probably understood through the chemically ordered network model and chemical bond approach[63] as described in the next paragraph.

The bonds of Se–Se (330.5 kJ mol^{-1}) are sturdier as compared to the bonds of Te–Te (293.3 kJ mol^{-1}).[64] Similarly, the Se atom has higher electro-negativity as compared to the Te atom. Thus, the bond strength of Se–Zn bonds is greater than Te–Zn bonds. Consequently, we can expect that zinc as a foreign element gives preference to Se after entering the glass network of parent glass and so there is a drop in the number of Se–Se bonds (330.5 kJ mol^{-1}) as an outcome of the dissolution of Zn atoms in polymeric Se-chains.[64] Thus, the creation of Se–Zn bond (170.7 kJ mol^{-1}) and Zn–Zn bonds (22 kJ mol^{-1}) occur.[64] Accordingly, the cohesive energy of the system decreases with a rise in the Zn concentration in the parent glass. This is probably the reason for the reduction in the overall value of mean bond energy and average heat of atomization of the preset samples with the rise in Zn concentration.

A crucial parameter to determine the permanency of glassy substances in the vitreous state is the released amount of the enthalpy (ΔH_{gc}) through the phase transformation from the non-crystalline state (*i.e.*, glassy phase) to the crystalline state (*i.e.*, crystal phase). It can be determined by subtracting the glass transition enthalpy (ΔH_g) from crystallization enthalpy (ΔH_c), so that:

$$\Delta H_{gc} = \Delta H_c - \Delta H_g \tag{19}$$

The glass having lower values of ΔH_{gc} possesses higher thermal stability. To confirm this, we have determined thermal stability by using the Saad–Poulin relation:[65]

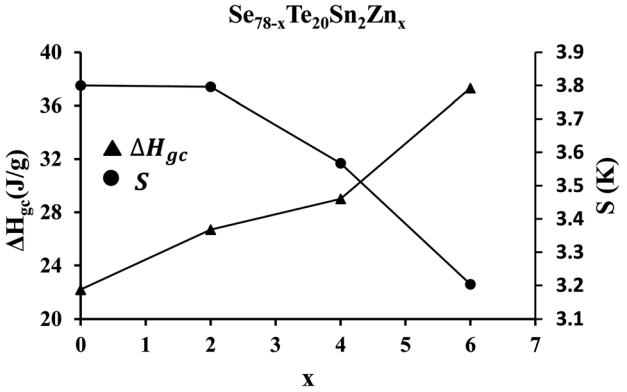

Fig. 10 Composition dependence of enthalpy (ΔH_{gc}) released during phase transformation from the glassy state to the crystalline state and thermal stability parameter S.

$$S = \frac{(T_c - T_o)(T_c - T_g)}{T_g} \quad (20)$$

Here T_o represent the on-set temperature of the crystallization peaks for the present samples. Knowing the values of stability parameter S, we have plotted the graphs of S and ΔH_{gc} against the composition of the zinc (see Fig. 10). The figure reveals that the thermal stability parameter S increases with decreasing ΔH_{gc}. A similar correlation was observed by Naqvi and Saxena in some samples of the glassy $Se_{80-x}Te_{20}Zn_x$ system.[66]

In the last two decades, various research groups have studied the thermal stability of zinc containing multicomponent (*i.e.*, binary, ternary, and quaternary) ChGs of Se–Te to optimize the durability and reduce aging effects.[22,66–68] Hence, we have compared the results of the present study with that are reported in ref. 22 and 66–68. The comparison of such data is tabulated in Table 3. This table reveals the better durability of the present samples as compared to others zinc containing multicomponent ChGs due to their thermal stability values.

Table 3 Comparisons of thermal stability for zinc containing ChGs in the present study and with the available data in literature

S. no.	Glass composition	S (K)	Reference
1	$Se_{98}Zn_2$	1.6	22
	$Se_{95}Zn_5$	2.7	
	$Se_{90}Zn_{10}$	2.5	
	$Se_{80}Zn_{20}$	2.0	
2	$Se_{70}Te_{28}Zn_2$	3.1	67
	$Se_{70}Te_{26}Zn_4$	3.6	
	$Se_{70}Te_{24}Zn_6$	2.9	
	$Se_{70}Te_{22}Zn_8$	3.3	
3	$Se_{78}Te_{20}Zn_2$	3.1	66
	$Se_{76}Te_{20}Zn_4$	3.2	
	$Se_{74}Te_{20}Zn_6$	2.9	
	$Se_{72}Te_{20}Zn_8$	2.4	
	$Se_{70}Te_{20}Zn_{10}$	1.9	
4	$Se_{93}Zn_2Te_5$	1.8	68
	$Se_{91}Zn_2Te_5In_2$	2.8	
	$Se_{89}Zn_2Te_5In_4$	3.9	
	$Se_{87}Zn_2Te_5In_6$	4.2	
	$Se_{83}Zn_2Te_5In_{10}$	3.0	
5	$Se_{78}Te_{20}Sn_2$	3.8	Present work
	$Se_{78}Te_{20}Sn_2Zn_2$	3.8	
	$Se_{76}Te_{20}Sn_2Zn_4$	3.7	
	$Se_{74}Te_{20}Sn_2Zn_6$	3.2	

4. Conclusions

The incorporation of zinc in SeTeSn helps in the synthesis of new third-generation samples of quaternary SeTeSnZn system that are free from the problem of phase separation. This is confirmed by the appearance of the sharp solo peaks at glass transition temperature in zinc-containing derived samples. Further analysis reveals that the activation energies corresponding to the crystallization and glass transition phenomena are decreased with a rise in the corresponding Lasocka parameters.

The crystallization rate is increased appreciably in the quaternary alloys after zinc incorporation in the parent SeTeSn ternary sample. The average heat of atomization and overall mean bond energy of the present samples is decreased with the reduction in cohesive energy when we increase the concentration of zinc. The thermal stability parameter is found to be increased with the drop in enthalpy released during the phase transformation from glass to the crystalline state.

Conflicts of interest

There are no conflicts to declare.

Acknowledgements

Neeraj Mehta is thankful to his university for providing an incentive under Institutions of Eminence (IoE) Scheme (Dev. Scheme No. 6031).

References

1 R. Gangadharan, V. Jayalakshmi, J. Kalaiselvi, S. Mohan, R. Murugan and B. Palanivel, Electronic and structural properties of zinc chalcogenides ZnX (X = S, Se, Te), *J. Alloys Compd.*, 2003, **359**, 22–26.
2 F. Janetzko and J. Karl, Miscibility of zinc chalcogenides, *J. Phys. Chem. A*, 2004, **108**, 5449–5453.
3 Y. Sun, Z. Sun, S. Gao, H. Cheng, Q. Liu, J. Piao, T. Yao, C. Wu, S. Hu, S. Wei and Y. Xie, Fabrication of flexible and freestanding zinc chalcogenide single layers, *Nat. Commun.*, 2012, **3**, 1057.
4 J. P. Dubey, R. Tiwari, K. S. Upadhyaya and P. K. Pandey, Crystal dynamics of zinc chalcogenides I: an application to ZnS, *Turk. J. Phys.*, 2015, **39**, 242–253.
5 J. P. Dubey, R. Tiwari, K. S. Upadhyaya and P. K. Pandey, Crystal dynamics of zinc chalcogenides II: an application to ZnSe, *IOSR J. Appl. Phys.*, 2015, **7**, 67–75.
6 J. P. Dubey, R. Tiwari, K. S. Upadhyaya and P. K. Pandey, Crystal dynamics of zinc chalcogenides III: an application to ZnTe, *Turk. J. Phys.*, 2016, **40**, 201–208.

7 J. Zhou, H. Zhuang and H. Wang, Layered tetragonal zinc chalcogenides for energy-related applications: from photocatalysts for water splitting to cathode materials for Li-ion batteries, *Nanoscale*, 2017, **9**, 17303–17311.
8 C. Tang, X. Wei, X. Cai, Q. An, P. Hu, J. Sheng, J. Zhu, S. Chou, L. Wu and L. Mai, ZnSe microsphere/multiwalled carbon nanotube composites as high-rate and long-life anodes for sodium-ion batteries, *ACS Appl. Mater. Interfaces*, 2018, **10**, 19626–19632.
9 S. Deb, P. K. Kalita and P. Datta, Opto-electronic characterization of starch capped zinc chalcogenides (core-shell) nanocomposites and their application as Schottky device, *Phys. Scr.*, 2020, **95**, 095810.
10 P. Li and T. He, Recent advances in zinc chalcogenide-based nanocatalysts for photocatalytic reduction of CO_2, *J. Mater. Chem. A*, 2021, **9**, 23364–23381.
11 R. Li, Y. Jiang, L. Xu, Z. Ma, F. Yang, J. Xu and W. Su, Enhanced threshold voltage of Zn-doped $Ge_2Sb_2Te_5$ phase-change memory deposited by electron-beam evaporation, *Phys. Status Solidi A*, 2013, **210**, 2650–2655.
12 Y. Chen, G. Wang, J. Li, X. Shen, T.-F. Xu, R. Wang, Y. Lu, X. Wang, S. Dai and Q. Nie, Sb-rich Zn–Sb–Te phase-change materials: a candidate for the trade-off between crystallization speed and data retention, *Appl. Phys. Express*, 2014, **7**, 105801.
13 G. Wang, X. Shen, Y. Lu, S. Dai, Q. Nie and T.-F. Xu, Understanding the role of Zn in improving the phase change behaviors of Sb_2Te_3 films, *Thin Solid Films*, 2015, **585**, 57–65.
14 Y. Chen, G. Wang, M. Tian, X. Shen, T.-F. Xu, Y. Lu, S. Dai and Q. Nie, Fast reversible laser-induced crystallization of Sb-rich Zn-Sb-Se phase change material with excellent stability, *AIP Adv.*, 2015, **5**, 077174.
15 G. Wang, H. Shi, A. Lotnyk, D. Shi and R. Wang, Conversion of p–n conduction type by spinodal decomposition in Zn-Sb-Bi phase-change alloys, *NPG Asia Mater.*, 2020, **12**, 17.
16 Z. Wang, G. Wang, Y. Luo, G. Chen, H. Wang, D. Shi, Y. Lu, K. Jiang, T. Gu and J. Zhong, Amorphous-to-crystalline phase transition in Ge-rich Ge-Te-Zn films with high thermal stability, *Vacuum*, 2016, **132**, 82–85.
17 J. Gu, Y. Chen, Q. Zhang, G. Wang, R. Wang, X. Shen, J. Wang and T. Xu, Crystallization kinetics with fragile-to-strong crossover in Zn-Sb-Te supercooled phase-change liquids, *Appl. Phys. Lett.*, 2019, **115**, 091903.
18 N. Mehta, K. Singh and N. S. Saxena, Comparative analysis of some thermo-physical properties of $Se_{90}Zn_{10}$ and $Te_{90}Zn_{10}$ alloys, *Thermochim. Acta*, 2008, **475**, 80–82.
19 S. Srivastava, N. Mehta, R. K. Shukla and A. Kumar, Effect of Zn incorporation on the a.c. conductivity of glassy $Se_{70}Te_{30}$ alloy, *Eur. Phys. J.: Appl. Phys.*, 2008, **44**, 217–221.
20 A. K. Singh and K. Singh, Crystallization kinetics and thermal stability of $Se_{98-x}Zn_2In_x$ chalcogenide glasses, *Philos. Mag.*, 2009, **89**, 1457–1472.
21 A. K. Singh, N. Mehta and K. Singh, Correlation between Meyer–Neldel rule and phase separation in $Se_{98-x}Zn_2In_x$ chalcogenide glasses, *Curr. Appl. Phys.*, 2009, **9**, 807–811.
22 M. Nasir, M. A. M. Khan, M. Husain and M. Zulfequar, Thermal properties of $Se_{100-x}Zn_x$ glassy system, *Mater. Sci. Appl.*, 2011, **2**, 289–298.
23 M. Nasir and M. Zulfequar, Estimation the density of localized state in glassy $Se_{100-x}Zn_x$ thin films by using space charge limited conduction measurement, *New J. Glass Ceram.*, 2012, **2**, 91–97.
24 M. Nasir and M. Zulfequar, DC conductivity and dielectric behaviour of glassy $Se_{100-x}Zn_x$ alloys, *Open J. Inorg. Non-Met. Mater.*, 2012, **2**, 11–17.
25 A. K. Singh, Comparative study on thermophysical properties of Se–Zn–In and Se–Zn–Te–In chalcogenide glasses, *Adv. Sci., Eng. Med.*, 2012, **4**, 123–127.
26 A. K. Singh, A comparative study on optical properties of Se–Zn–In and Se–Zn–Te–In chalcogenide glasses, *Optik*, 2013, **124**, 2187–2190.
27 S. N. Kishore, R. Kundu and S. Dhankhar, FTIR and optical properties of various Se-S-Zn chalcogenide glasses, *IOP Conf. Ser.: Mater. Sci. Eng.*, 2015, **73**, 012150.
28 S. Ahmad, M. Nasir, K. Asokan, M. S. Khan and M. Zulfequar, Electronic excitation induced structural, optical and electrical properties of $Se_{85}S_{10}Zn_5$ thin films and applicability of a single oscillator model, *RSC Adv.*, 2015, **5**, 69400–69409.
29 G. Abbady, K. Aly, Y. Saddeek and N. Afifiy, Linear and non-linear optical properties of amorphous Se and M_5Se_{95} (M = Ge, Ga and Zn) films, *Bull. Mater. Sci.*, 2016, **399**, 1819–1825.
30 A. Alwany, M. Algradee, M. M. Hafith and M. Abdel-Rahim, Structural and optical properties of $Ge_{20}Se_{70}Zn_{10}$ thin films, *Int. J. Sci. Eng. Investig.*, 2017, **6**, 90–97.
31 X. Lu, Y. Zhang, J. Ren, E. Lewis, G. Farrell, A. Yang, Z. Yang and P. Wang, Chalcogenide glasses with embedded ZnS nanocrystals: potential mid-infrared laser host for divalent transition metal ions, *J. Am. Ceram. Soc.*, 2018, **101**, 666–673.
32 Y. Azhniuk, D. Solonenko, E. Sheremet, V. Dzhagan, V. Loya, I. V. Grytsyshche, S. Schulze, M. Hietschold, A. V. Gomonnai and D. Zahn, Structural and optical study of Zn-doped As_2Se_3 thin films: evidence for photoinduced formation of ZnSe nanocrystallites, *AIP Adv.*, 2019, **9**, 065212.
33 G. Nagpal, I. Sharma and S. K. Tripathia, The effect of substitution of Sb with Zn on the optical and physical properties of $Se_{90}Sb_{10-x}Zn_x$ (x = 0, 2, 4, 6, 10 at. %) thin films, *Optik*, 2020, **207**, 164460.
34 M. Chazot, C. Arias, M. Kang, C. Blanco, A. Kostogiannes, J. Cook, A. Yadav, V. Rodriguez, F. Adamietz, D. Verreault, S. Danto, T. Loretz, A. Seddon, D. Furniss, K. Schepler, M. Richardson and K. Richardson, Investigation of ZnSe stability and dissolution behavior in As-S-Se chalcogenide glasses, *J. Non-Cryst. Solids*, 2021, **555**, 120619.
35 A. Velea, F. Sava, P. Badica, M. Burdusel, C. Mihai, A. Galca, E. Matei, A. Buruiana, O. El Khouja and L. Calvez, New chalcogenide glass-ceramics based on Ge-Zn-Se for IR applications, *Materials*, 2022, **18**, 5002.
36 T. Bennett, Y. Yue, P. Li, A. Qiao, H. Tao, N. G. Greaves, T. Richards, G. I. Lampronti, S. A. T. Redfern, F. Blanc, O. Farha, J. Hupp, A. Cheetham and D. Keen, Melt-

Quenched Glasses of Metal–Organic Frameworks, *J. Am. Chem. Soc.*, 2016, **138**, 3484–3492.

37 C. Qiao, Y. R. Guo, F. Dong, J. Wang, H. Shen, S. Wang, M. Xu, X. Miao, Y. Zheng, R. Zhang, L. Chen, C. Wang and K. Ho, Evolution of short and medium-range order in the melt-quenching amorphization of $Ge_2Sb_2Te_5$, *J. Mater. Chem. C*, 2018, **6**, 5001–5011.

38 M. C. Brand, F. Greenwell, R. Clowes, B. D. Egleston, A. Kai, A. Cooper, T. Bennett and R. L. Greenaway, Melt-quenched porous organic cage glasses, *J. Mater. Chem. A*, 2021, **9**, 19807–19816.

39 N. Mehta, Characterization techniques for the study of thermally activated phase transitions and determination of thermo-physical/kinetic properties, in *Advanced Analytic and Control Techniques for Thermal Systems with Heat Exchangers*, ed. L. Pekar, Elsevier, 2020, pp. 149–166.

40 C. Jijian, Phase separation and crystallization of chalcogenide glass-forming systems, *J. Non-Cryst. Solids*, 1993, **161**, 304–308.

41 N. Mehta and A. Kumar, Observation of phase separation in some Se–Te–Ag chalcogenide glasses, *Mater. Chem. Phys.*, 2006, **96**, 73–78.

42 S. Stehlík, J. Kolar, H. Haneda, I. Sakaguchi, M. Frumar and T. Wagner, Phase separation in chalcogenide glasses: the system AgAsSSe, *Int. J. Appl. Glass Sci.*, 2011, **2**, 301–307.

43 F. Abdel-Wahab, Observation of phase separation in some Se–Te–Sn chalcogenide glasses, *Phys. B*, 2011, **406**, 1053–1059.

44 M. Lasocka, The effect of scanning rate on glass transition temperature of splat-cooled $Te_{85}Ge_{15}$, *Mater. Sci. Eng.*, 1976, **23**, 173–177.

45 W. Kauzmann, The nature of the glassy state and the behavior of liquids at low temperatures, *Chem. Rev.*, 1948, **43**, 219–256.

46 T. Ichitsubo, E. Matsubara, H. Numakura, K. Tanaka, N. Nishiyama and R. Tarumi, Low-temperature elastic moduli of a Pd-based metallic glass showing positive phonon dispersion, *Phys. Rev. B: Condens. Matter Mater. Phys.*, 2005, **72**, 052201.

47 D. Selvanathan, W. J. Bresser and P. Boolchand, Stiffness transitions Si_xSe_{1-x} in glasses from Raman scattering and temperature-modulated differential scanning calorimetry, *Phys. Rev. B: Condens. Matter Mater. Phys.*, 2000, **61**, 15061.

48 P. Boolchand, D. G. Georgiev and B. Goodmana, Discovery of the intermediate phase in chalcogenide glasses, *J. Optoelectron. Adv. Mater.*, 2001, **3**, 703–720.

49 D. G. Georgiev, P. Boolchand and M. Micoulaut, Rigidity Transitions and Molecular Structure of As_xSe_{1-x} Glasses, *Phys. Rev. B: Condens. Matter Mater. Phys.*, 2000, **62**, 9228.

50 J. C. Phillips, Topology of covalent non-crystalline solids i: short-range order in chalcogenide alloys, *J. Non-Cryst. Solids*, 1979, **34**, 153–181.

51 S. O. Kasap, D. Tonchev and T. Wagner, Heat capacity and the structure of chalcogenide glasses studied by temperature-modulated differential scanning calorimetry, *J. Mater. Sci. Lett.*, 1998, **17**, 1809–1811.

52 S. Saraswat and S. S. S. Kushwaha, Structural interpretation of specific heat measurements on glassy $Se_{100-x}Sb_x$ alloys, *Philos. Mag.*, 2009, **89**, 583–593.

53 C. T. Moynihan, A. J. Easteal, J. Wilder and J. Tucker, Dependence of the glass transition temperature on heating and cooling rate, *J. Phys. Chem.*, 1974, **78**, 2673–2677.

54 H. E. Kissinger, Reaction kinetics in differential thermal analysis, *Anal. Chem.*, 1957, **29**, 1702–1706.

55 H. Kumar, N. Mehta and K. Singh, Calorimetric studies of glass transition phenomenon in glassy $Se_{80-x}Te_{20}Sn_x$ alloys, *Phys. Scr.*, 2009, **80**, 065602.

56 K. Matusita and S. Sakka, Kinetic study of the crystallization of glass by differential scanning calorimetry, *Phys. Chem. Glasses*, 1979, **20**, 81–84.

57 K. Matusita and S. Sakka, Study of non-isothermal crystallization of glass by thermal analysis, *Bull. Inst. Chem. Res.*, 1981, **59**, 159–171.

58 J. Augis and J. Bennett, Calculation of the Avrami parameters for heterogeneous solid state reactions using a modification of the Kissinger method, *J. Therm. Anal. Calorim.*, 1978, **13**, 283–292.

59 S. Arrhenius, About the rate of reaction in the inversion of cane sugar by acids, *Z. Phys. Chem.*, 1889, **4**, 226–248.

60 S. Arrhenius, About the dissociation of water dissolved substances, *Z. Phys. Chem.*, 1887, **1**, 631–648.

61 N. Chandel and N. Mehta, Analysis of physicochemical properties in covalent network chalcogenide glasses (ChGs): critical review of theoretical modeling of chemical bond approach, *SN Appl. Sci.*, 2019, **1**, 657.

62 L. Tichy and H. Ticha, Covalent bond approach to the glass-transition temperature of chalcogenide glasses, *J. Non-Cryst. Solids*, 1995, **189**, 141–146.

63 N. Mehta and A. Kumar, Thermal characterization of glassy $Se_{70}Te_{20}M_{10}$ using DSC technique, *J. Mater. Sci.*, 2004, **39**, 6433–6437.

64 W. M. Haynes and D. R. Lide, *CRC Handbook of Chemistry and Physics*, section 9, 2014, pp. 65–69.

65 M. Saad and M. Poulin, Glass forming ability criterion, *Mater. Sci. Forum*, 1987, **19–20**, 11–18.

66 S. Faheem Naqvi and N. S. Saxena, Role of additive (Zn) incorporation on the glass/crystal thermodynamics and stability of $Se_{80-x}Te_{20}Zn_x$ (x = 2, 4, 6, 8 and 10) glassy alloys, *J. Non-Cryst. Solids*, 2011, **357**, 1804–1810.

67 S. Srivastava, M. Zulfequar and A. Kumar, Glass transition kinetics of some $Se_{70}Te_{30-x}Zn_x$ chalcogenide glasses, *J. Ovonic Res.*, 2008, **4**, 1–11.

68 A. K. Singh, N. Mehta and K. Singh, Effect of indium additive on glass-forming ability and thermal stability of Se-Zn-Te chalcogenide glasses, *Philos. Mag. Lett.*, 2010, **90**, 201–208.